

Adiabatically tuning quantized supercurrents in an annular Bose-Einstein condensate

Junpeng Hou, Xi-Wang Luo, Kuei Sun, and Chuanwei Zhang*

Department of Physics, The University of Texas at Dallas, Richardson, Texas 75080-3021, USA

The ability to generate and tune quantized persistent supercurrents is crucial for building superconducting or atomtronic devices with novel functionalities. In ultracold atoms, previous methods for generating quantized supercurrents are generally based on dynamical processes to prepare atoms in metastable excited states. Here we show that arbitrary quantized circulation states can be adiabatically prepared and tuned as the ground state of a ring-shaped Bose-Einstein condensate by utilizing spin-orbital-angular-momentum (SOAM) coupling and an external potential. There exists superfluid hysteresis for tuning supercurrents between different quantization values with nonlinear atomic interactions, which is explained by developing a nonlinear Landau-Zener theory. Our work will provide a powerful platform for studying SOAM coupled ultracold atomic gases and building novel atomtronic circuits.

Introduction. Quantized supercurrents are one of the most remarkable phenomena of superfluids and superconductors and have been widely studied in solid-state superconductors [1] and ultracold atomic gases [2, 3]. Such persistent circulation currents are crucial elements for building many important devices such as SQUID [4–6], superfluid gyroscopes [7–9], atomic interferometers [10–14] and atomtronic circuits [15, 16]. These important applications naturally require the experimental ability of coherent generation and manipulation of quantized supercurrents. In this context, ultracold atomic gases possess intrinsic advantages for unprecedented control of experimental parameters and the lack of disorder [17].

Great progresses have been made recently for generating quantized circulation supercurrents in a ring-shaped geometry and exploring these properties and device applications [2, 18–25]. So far two experimental tools have been applied to prepare quantized circulation currents for an annular Bose-Einstein condensate (BEC): *i*) a short two-photon Raman pulse with orbital angular momentum (OAM) transfer between two spin states [2, 20, 21] using Laguerre-Gaussian (LG) laser beams [26]; *ii*) periodic rotation of a local repulsive potential barrier along a ring [22–25]. These methods involve dynamical process to transfer atoms to metastable high OAM states [see Fig. 1 (c)], which could induce complicated excitations, heating, and decays of the BEC. Therefore a nature question is whether quantized supercurrents can be adiabatically prepared and manipulated as the ground state of an annular BEC to circumvent these issues.

To prepare a finite OAM circulation state as the ground state, the OAM need be coupled with other degrees of freedom such as spins, as we see from the spin-orbit coupling [27–34]. Recently, spin–OAM (SOAM) coupling has been proposed for ultracold atoms using LG Raman lasers with finite OAM to couple two atomic hyperfine spin states [35–37]. Since OAM is still a good quantum number on a ring, an external nonuniform potential is needed to induce coupling between different OAM states.

In this Letter, we show that the combination of these

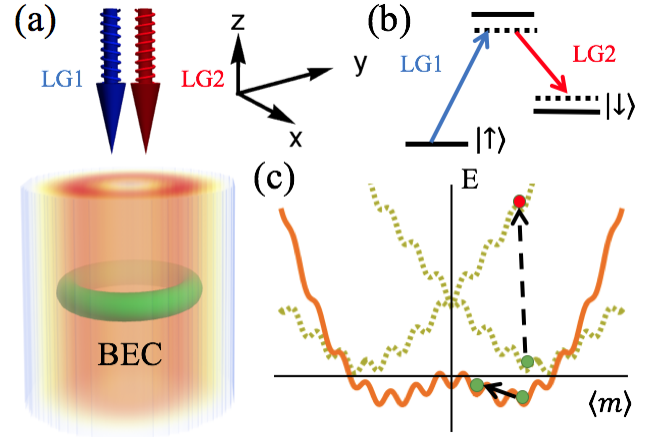


FIG. 1. (Color online) (a) Experimental scheme to generate a SOAM-coupled ring BEC with co-propagating LG beams. (b) Raman transition induced by the LG beams. (c) Schematic plot of the energy spectrum vs average quasi-OAM number m with and without Raman coupling (solid and dashed curves, respectively). The energy barriers between integer m are due to nonlinear interactions. Green (red) circles denote ground (excited) states. Previous experiments using a Raman short pulse dynamically excite the BEC to an upper metastable state (dashed arrow) [2, 20, 21]. While in our scheme the system remains on the ground state during the adiabatic process (solid arrows).

two ingredients, SOAM coupling and nonuniform potential, allows adiabatic preparation and control of quantized supercurrents with arbitrary OAM as the system ground state in a ring-shaped BEC. Our main results are:

i) A circulation state with arbitrary OAM can be generated on demand with a high precision from a non-rotating state at a time scale $\sim 10\hbar/E_R$, where $E_R = \hbar^2/2MR^2$ is the energy unit defined by atomic mass M and ring radius R . Large interaction strength or OAM states shorten the time required for the adiabatic process. Such circulation state carries both non-zero particle and spin supercurrents. Because the adiabatic preparation

process is free from complicated excitations and the system is on ground state, the generated quantized supercurrents are stable against heating and decaying of the BEC.

ii) The tuning of supercurrents between different circulation states strongly depends on the interatomic interaction and nonuniform potential, which, in a proper parameter region, possesses superfluid hysteresis.

iii) We develop a nonlinear Landau-Zener theory to explain the observed adiabatic preparation and superfluid hysteresis, which exhibits a swallowtail energy structure due to nonlinear interactions.

Model and Hamiltonian. We consider an atomic BEC with two internal spin states $(\psi_\uparrow \ \psi_\downarrow)^T$, subject to a pair of co-propagating vertical LG beams with opposite OAM number $\pm l$ [see Fig. 1(a)] and $\Omega_\pm(r) = \Omega_0 \left(\frac{\sqrt{2}r}{w}\right)^{|l|} \exp\left(-\frac{r^2}{w^2} \pm il\phi - ik_L z\right)$, where (r, ϕ, z) are cylindrical coordinates, and Ω_0 , w , and k_L are the beams' amplitude, waist, and wavevector in the \hat{z} direction, respectively. The LG beams induce a Raman transition [as in Fig. 1(b)] that generates the SOAM coupling [35–37]. An additional far-detuned vertical LG laser with the same beam waist and OAM provides the tube potential around the maximum beam intensity $r = \sqrt{l/2}w$ and a horizontal “sheet” beam provides the confinement along the z direction [21]. Together the SOAM-coupled BEC is confined on an annular geometry of a fixed radius R and can be described by an effective single-particle Hamiltonian [35] in units of E_R and \hbar ($= 1$), as

$$H_0^{\text{ring}} = -\partial_\phi^2 + (2il\partial_\phi + \delta/2)\sigma_z + \Omega\sigma_x, \quad (1)$$

plus interatomic interactions. Here δ is the Zeeman detuning, Ω is the Raman coupling strength, and $\{\sigma\}$ are the Pauli matrices.

The Hamiltonian has two energy bands. The eigenstates of the lower band are plane waves in the $\hat{\phi}$ direction $|m\rangle = (\cos\theta_m, -\sin\theta_m)^T e^{im\phi}$, where m is an integer due to the periodic boundary condition. Note that m represents a quasi-OAM quantum, while the up and down components have real OAM $\propto (m \mp l)$ [35], respectively. In other words, the $|m\rangle$ state physically carries quantized particle supercurrent $J_c(m) = m - l \cos 2\theta_m$ and spin supercurrent $J_s(m) = m \cos 2\theta_m - l$. The ground-state supercurrent configurations change with Ω . Given $\delta = 0$ and $\Omega = 0$, the lower band has two degenerate minima at $m = \pm l$ [as in Fig. 1(c)]. As Ω increases, the double minima shift toward each other and merge at $m = 0$ when $\Omega = 4l^2 - 1$, above which the band has a single minimum $m = 0$. In the double-minima region, any pair of $|\pm m\rangle$ states exhibits a Z_2 symmetry by having opposite spin polarization $\langle\sigma_z\rangle = \cos 2\theta_m$, opposite J_c , and same J_s . Below we focus on the plane-wave state on the $m \geq 0$ side.

Preparation of quantized supercurrent. To create the ground state or manipulate the supercurrent circulation

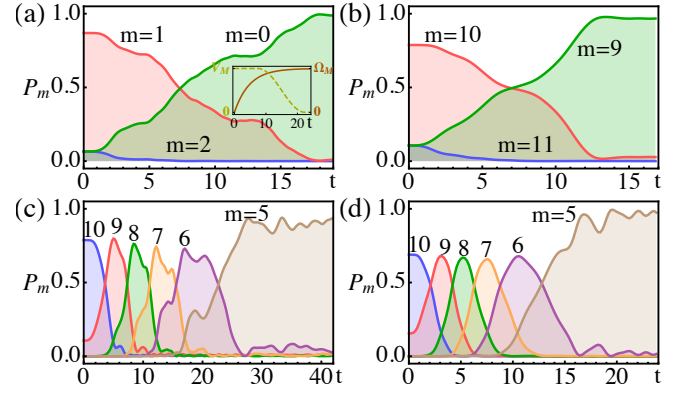


FIG. 2. (Color online) Time evolution of the BEC’s population at $|m\rangle$, or P_m , under the simultaneous increase in Ω and decrease in V (solid and dashed curves in the inset, respectively). (a) Loading the BEC to $|0\rangle$ from an initially prepared state with potential $V_M = 3$. The system parameters are $l = 1$, $\Omega_M = 3$, $g_{\uparrow\uparrow} = 15$, and $g_{\downarrow\downarrow} = g_{\uparrow\downarrow} = 0.9954g_{\uparrow\uparrow}$. (b) Loading to $|9\rangle$ with higher LG beams $l = 10$ and stronger $\Omega_M = 70$ in a similar procedure. (c) Same initial state as (b), but the BEC transfers across multiple states to $|5\rangle$ (with $\Omega_M = 180$). (d) Same as (c) except stronger $g_{\uparrow\uparrow} = 60$ and $V_M = 15$.

in the ring system, one may properly tune Ω to load the BEC at a desired quantum m , as it naturally pursues the energy minimum. However, there are two issues preventing this. First, all m states are stationary states and do not couple to each other, so a high- m state can have a very long lifetime. Second, a smooth transition between adjacent m states encounters an energy barrier induced by interatomic interaction, which takes the form of

$$E_g = \frac{1}{2\pi} \int_0^{2\pi} (g_{\uparrow\uparrow}|\psi_\uparrow|^4 + g_{\downarrow\downarrow}|\psi_\downarrow|^4 + 2g_{\uparrow\downarrow}|\psi_\uparrow|^2|\psi_\downarrow|^2) d\phi. \quad (2)$$

In Fig. 1(c), we schematically plot the system energy vs expectation value of m for a superposition of two adjacent $|m\rangle$ states. The ripples reflect the interaction effects: the local minima correspond to pure $|m\rangle$ states, while the local maxima correspond to the equal superposition of two adjacent $|m\rangle$ states, which possess density modulations that cost interaction energy.

To assist the BEC to overcome the barrier and move toward a lower energy state, it is essential to trigger sufficient coupling between adjacent $|m\rangle$ states. We propose the use of a linear external potential $V_{\text{ext}} = V(t)x/R = V(t)\cos\phi$, which couples two states as $\langle m| \cos\phi |m\pm 1\rangle = \frac{1}{2}\langle m|e^{i\phi} + e^{-i\phi}|m\pm 1\rangle \neq 0$. Such potential has already been experimentally applied to annular BECs without SOAM coupling [38]. In addition, one can use the linear slope around $x = 0$ for a Gaussian laser $V(x) = V_0 \exp(-(x-\xi)^2/2\xi^2) \approx V_0 \exp(-1/2)(1+x/\xi)$ with $\xi \gg R$. We propose a process of tuning both Ω and V simultaneously, as illustrated in the inset of Fig. 2(a), and simulate the system evolution with the time-dependent

Gross-Pitaevskii equation (GPE). Initially, the BEC is prepared in the presence of external potential $V(0) = V_M$. The Raman coupling Ω is then slowly ramped on to shift the band minimum, while V is gradually turned off to suppress the coupling. Finally, at $\Omega(t) = \Omega_M$ and $V(t) = 0$, the BEC stays in the new ground state, the targeted single- m state, which decouples from the others and carries the aforementioned particle and spin supercurrents.

Our simulation of four different cases is presented in Fig. 2. We plot the BEC's population P_m at several associated m states as a function of time. In panel (a) for $l = 1$, the BEC starts from a $|1\rangle$ dominant state and ends at an almost single- m state, $|0\rangle$, demonstrating an effective transfer between adjacent states. Although the initial state also couples to $|2\rangle$, the BEC clearly pursues the lower energy state $|0\rangle$. In general, higher energy states are hardly involved during the transition. The same procedure can be applied to a large $l = 10$, as shown in Fig. 2(b), where only Ω_M is changed for the desired band minimum. The system actually undergoes a smoother transition with a shorter transition time for a large l . Using the same strategy, one may possibly reach any m state ($0 \leq m \leq l$) by repeating the Ω and V cycle to lower the m number one by one. However, such a transfer, e.g. from $|10\rangle$ to $|5\rangle$, can be achieved with a single process and hence in a shorter time [see Fig. 2(c)]. The BEC passes through multiple m states with each intermediate m state dominating in a narrow time window, and stops at the final m state. In Fig. 2(d), we quadruple the interatomic interaction and increase V_M accordingly to overcome the interaction energy barrier. The transition goes more smoothly and the transition time is significantly shorter.

Superfluid hysteresis. Hysteresis is a hallmark phenomena of quantized supercurrents [39–41], and recently a hysteresis loop for supercurrent jumps in an annular BEC has been observed in experiments, where a periodically rotating local laser barrier is used to induce the transition [25]. In our system, the supercurrent change is driven by the SOAM coupling to change the ground state, which, unlike the local laser barrier, acts on the whole system uniformly. Below we will show the existence of superfluid hysteresis using numerical GPE simulation (Fig. 3), followed by developing a nonlinear Landau-Zener theory [42–44] to explain the physics, where a swallowtail band structure is ascribed to the origin of the observed hysteretic phenomenon.

The time procedure of $\Omega(t)$ and $V(t)$ in our simulation is illustrated in Fig. 3(a) inset. In the forward evolution, $\Omega(t)$ linearly increases from Ω_m to Ω_M with the initial ground state prepared at Ω_m , while $V(t)$ is turned on up to the maximum V_M and then symmetrically turned off. In the backward evolution, $\Omega(t)$ and $V(t)$ take the time-reversal path, with the initial ground state prepared at Ω_M . Since $V(t)$ is the key ingredient that induces the

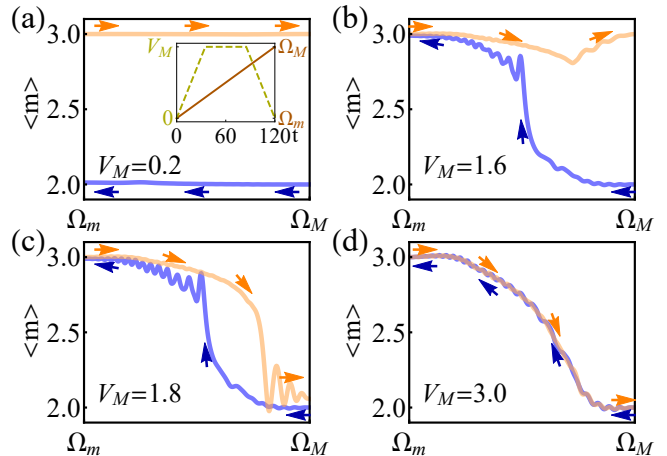


FIG. 3. (Color online) Inner panel shows time procedure of $\Omega(t)$ (solid curve, axis on the right) and $V(t)$ (dashed curve, axis on the left) for studying the superfluid hysteresis. The Raman coupling Ω_m (Ω_M) corresponds to the ground state being $|3\rangle$ ($|2\rangle$). (a)–(d) Time evolution of the expectation value $\langle m \rangle$ shows no transition at $V_M = 0.2$, single-side transition at $V_M = 1.6$, a hysteretic loop at $V_M = 1.8$, and a loop without hysteresis at $V_M = 3$, respectively. The forward evolution (orange curve) starts from $|3\rangle$, and the reversal (blue curve) starts from $|2\rangle$, with both directions indicated by the arrows.

transition, we expect that it plays a crucial role on the hysteresis phenomenon. In Fig. 3(a)–(d), we plot the expectation value $\langle m \rangle$ for transitions between $|2\rangle$ and $|3\rangle$ at various V_M . At weak $V_M = 0.2$, there is no transition [Fig. 3(a)]. At $V_M = 1.6$ [Fig. 3(b)], the system cannot jump from $|3\rangle$ to $|2\rangle$ before the coupling is turned off, leaving the path unclosed. With the increase of the potential to $V_M = 1.8$ [Fig. 3(c)], a two-way transition happens with a clear hysteresis loop. At a strong $V_M = 3$ [Fig. 3(d)], the coupling completely overwhelms the barrier, and the loop becomes trivial, as the system follows the same path forward and backward.

The above observed phenomena can be intuitively illustrated from a double well energy structure [Fig. 4(a1)] in proper phase space of parameters of the system. Initially, BEC always stays in one of the minimum (ground state). During the evolution, the energy difference Δ_Ω between the two minima changes with $\Omega(t)$, while the barrier height Δ_V is determined by the interaction and $V(t)$. If V_M is sufficiently weak, the two minima are well separated by the barrier, and the hopping h_V is not strong enough to overcome it. As a result, the BEC is trapped in one minimum without any transition. As V_M increases, the minimum on which the BEC originally stays disappears during the process, and the BEC jumps to the other minimum. Such evolution is not symmetric in the time-reversal path, leading to the hysteretic behavior [Fig. 3(c)]. If V_M is strong, the initial minimum continuously evolves to the final minimum, and vice versa, resulting in the trivial loop [Fig. 3(d)].

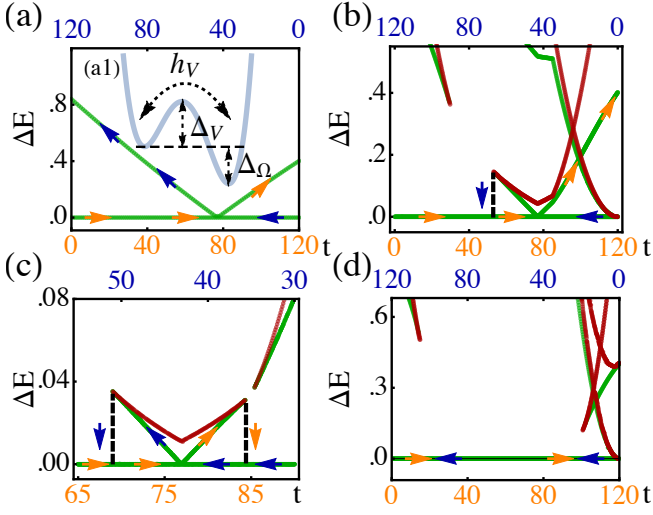


FIG. 4. (color online) (a1) Schematic plot of the double-well structure of the system in the phase space, characterized by the energy difference between the two minima Δ_Ω , barrier height Δ_V , and hopping strength h_V . (a)–(d) Energy band structure during the evolution in Fig. 3(a)–(d), respectively. The green and red curves represent the band minima and maxima (or saddle points), respectively. The arrows indicate the evolution direction, same as in Fig. 3, and the dashed lines indicate the sudden jump to ground states. Panel (c) is rescaled to emphasize the swallow-tail structure, which explains how the transitions happen differently between the forward and backward evolutions, resulting in the superfluid hysteresis.

This intuitive picture is confirmed by developing a nonlinear Landau-Zener theory for our system. As shown in Fig. 2, the transition process between $|m\rangle$ and $|m-1\rangle$ barely involves other higher-energy states, which allows us to build an effective Hamiltonian in a truncated space spanned by two relevant quasi-OAM and two spin states. The system's wavefunction is determined by four complex amplitudes as $\begin{pmatrix} a_1 \\ a_2 \end{pmatrix} e^{i(m-1)\phi} + \begin{pmatrix} a_3 \\ a_4 \end{pmatrix} e^{im\phi}$, subject to a normalization condition $\sum_{j=1}^4 p_j = 1$ with $p_j = |a_j|^2$.

Following the general formalism for nonlinear Landau-Zener tunneling [43, 44], we construct a semi-classical Hamiltonian with canonical coordinates ($q_j = \arg a_j, p_j$)

$$\begin{aligned} \mathcal{H} = & (l-m+1)^2 p_1 + (l-m)^2 p_3 + (l+m-1)^2 p_2 + \\ & (l+m)^2 p_4 + 2V[\sqrt{p_1 p_3} \cos(q_1 - q_3) + \sqrt{p_2 p_4} \cos q_2] + \\ & 2\Omega[\sqrt{p_1 p_2} \cos(q_1 - q_2) + \sqrt{p_3 p_4} \cos q_3] + \\ & (g/\pi)[p_1 p_3 + p_2 p_4 + \sqrt{p_1 p_2 p_3 p_4} \cos(q_1 - q_2 - q_3)], \quad (3) \end{aligned}$$

with a global phase chosen for $q_4 = 0$ and $g = g_{\uparrow\uparrow} = g_{\downarrow\downarrow} = g_{\downarrow\uparrow}$.

For each $\Omega(t)$ and $V(t)$ during the transition, we can find a global energy minimum (ground-state energy) in the phase space formed by six parameters (p_i, q_i) ($i = 1, 2, 3$). There also exist other interaction-induced

local energy minima, as shown in the energy structure in Fig. 4(a)–(d), with parameters corresponding to Fig. 3(a)–(d), respectively. In particular, a double-well structure with the emergence of two energy minima similar as Fig. 4(a1) is observed in the phase space (see Supplementary Materials), which confirms the above intuitive explanation of the hysteretic behavior. Because of multiple local energy minima for the same parameter, the energy band structure in Fig. 4 shows swallow-tail shape in proper parameter region. In Fig. 4(a), two bands simply cross and both minima survive during the procedure. As a result, the condensate remains on its initial minimum, which ends as a metastable state, without undergoing a transition [Fig. 3(a)]. With larger potential [Fig. 4(b)], only the left-hand-side band minimum breaks. Therefore, when starting from $|2\rangle$, the minimum disappears after the cross, forcing BEC to drop to the ground state. This result agrees with the GPE simulation in Fig. 3(b). With a deeper trap, the breakdown of band minimum is symmetric [Fig. 4(c)], therefore abrupt changes in $\langle m \rangle$ happen in both directions, yielding the hysteresis loop observed in Fig. 3(c). After V_M exceeds some critical value, the barrier vanishes and the BEC always stays on the ground state [Fig. 4(d)]. Therefore the system follows exactly the same path during the evolution as observed in Fig. 3(d). Our quantized supercurrent preparation should use this parameter region.

Experimental consideration. In experiments, we can consider a ^{87}Rb gas [22, 23] trapped in a ring of radius $R = 8 \mu\text{m}$, and use LG beams $l = 10$ [20]. The energy unit $E_R = 2\pi\hbar \times 0.924 \text{ Hz}$. For the transition procedure ($|10\rangle$ to $|5\rangle$) shown in Fig. 2 (d), $\Omega_M = 2\pi\hbar \times 166 \text{ Hz}$, $V_M = 2\pi\hbar \times 14 \text{ Hz}$ and the overall time length $T = 3.4 \text{ s}$. For a small Raman coupling strength Ω_M around 1 kHz, the heating effect can be neglected within a timescale of few seconds [45]. Considering the same configuration but with ^{23}Na [46], the parameters become $E_R = 2\pi\hbar \times 3.434 \text{ Hz}$, $\Omega_M = 2\pi\hbar \times 618 \text{ Hz}$, $V_M = 2\pi\hbar \times 52 \text{ Hz}$, $T = 0.9 \text{ s}$.

Conclusion. We have proposed a method to adiabatically prepare and tune arbitrary quantized circulation states as the ground states of an annular BEC, which carry both quantized atom and spin supercurrents. The whole procedure can be achieved at a time scale $\sim 10\hbar/E_R$ with a satisfactory fidelity. Our system provides a powerful platform for studying phenomena and applications of quantized supercurrents, exploring physics of SOAM coupled atomic gases, and building atomtronic devices with novel functionalities.

Acknowledgements: This work is supported by AFOSR (FA9550-16-1-0387), NSF (PHY-1505496), and ARO (W911NF-17-1-0128).

* Corresponding author.

Email: chuanwei.zhang@utdallas.edu

- [1] M. Tinkham, Introduction to Superconductivity, 2nd Ed. Dover Publications (2004).
- [2] C. Ryu, M. F. Andersen, P. Clade, V. Natarajan, K. Helmerson, and W. D. Phillips, Observation of Persistent Flow of a Bose-Einstein Condensate in a Toroidal Trap, *Phys. Rev. Lett.* **99**, 260401 (2007).
- [3] L. Corman, L. Chomaz, T. Bienaime, R. Desbuquois, C. Weitenberg, S. Nascimbene, J. Dalibard, and J. Beugnon, Quench-Induced Supercurrents in an Annular Bose Gas, *Phys. Rev. Lett.* **113**, 135302 (2014).
- [4] C. Ryu, P. W. Blackburn, A. A. Blinova, and M. G. Boshier, Experimental Realization of Josephson Junctions for an Atom SQUID, *Phys. Rev. Lett.* **111**, 205301 (2013).
- [5] Y. Sato and R. E. Packard, Superfluid helium quantum interference devices: physics and applications, *Rep. Prog. Phys.* **75**, 016401 (2012).
- [6] J. Clarke and A.I. Braginski, The SQUID Handbook (Wiley-VCH, Weinheim, 2004), Vols. 1-2.
- [7] R. E. Packard and S. Vitale, Principles of superfluid-helium gyroscopes, *Phys. Rev. B* **46**, 3540 (1992).
- [8] K. Schwab, N. Bruckner, and R. E. Packard, Detection of the Earth's rotation using superfluid phase coherence, *Nature (London)* **386**, 585 (1997).
- [9] T. L. Gustavson, P. Bouyer, and M. A. Kasevich, Precision Rotation Measurements with an Atom Interferometer Gyroscope, *Phys. Rev. Lett.* **78**, 2046 (1997).
- [10] M. Kasevich and S. Chu, Atomic interferometry using stimulated Raman transitions, *Phys. Rev. Lett.* **67**, 181 (1991).
- [11] R. Mathew, A. Kumar, S. Eckel, F. Jendrzejewski, G. K. Campbell, Mark Edwards, and E. Tiesinga, Self-heterodyne detection of the in situ phase of an atomic superconducting quantum interference device, *Phys. Rev. A* **92**, 033602 (2015).
- [12] G. E. Marti, R. Olf, and D. M. Stamper-Kurn, Collective excitation interferometry with a toroidal Bose-Einstein condensate, *Phys. Rev. A* **91**, 013602 (2015).
- [13] E. Hoskinson, Y. Sato, and R. Packard, Superfluid 4He interferometer operating near 2K, *Phys. Rev. B* **74**, 100509 (2006).
- [14] R. W. Simmonds, A. Marchenkov, E. Hoskinson, J. C. Davis, and R. E. Packard, Quantum interference of superfluid 3He, *Nature (London)* **412**, 55 (2001).
- [15] B. T. Seaman, M. Kramer, D. Z. Anderson, and M. J. Holland, Atomtronics: Ultracold-atom analogs of electronic devices, *Phys. Rev. A* **75**, 023615 (2007).
- [16] R. A. Pepino, J. Cooper, D. Z. Anderson, and M. J. Holland, Atomtronic Circuits of Diodes and Transistors, *Phys. Rev. Lett.* **103**, 140405 (2009).
- [17] I. Bloch, J. Dalibard, and W. Zwerger, Many-body physics with ultracold gases, *Rev. Mod. Phys.* **80**, 885 (2008).
- [18] K.-P. Marzlin, W. Zhang, and E. M. Wright, Vortex Coupler for Atomic Bose-Einstein Condensates, *Phys. Rev. Lett.* **79**, 4728 (1997).
- [19] N. R. Cooper and Z. Hadzibabic, Measuring the Superfluid Fraction of an Ultracold Atomic Gas, *Phys. Rev. Lett.* **104**, 030401 (2010).
- [20] S. Moulder, S. Beattie, R. P. Smith, N. Tammuz, and Z. Hadzibabic, Quantized supercurrent decay in an annular Bose-Einstein condensate, *Phys. Rev. A* **86**, 013629 (2012).
- [21] S. Beattie, S. Moulder, R. J. Fletcher, and Z. Hadzibabic, Persistent Currents in Spinor Condensates, *Phys. Rev. Lett.* **110**, 025301 (2013).
- [22] A. Ramanathan, K. C. Wright, S. R. Muniz, M. Zelan, W. T. Hill, C. J. Lobb, K. Helmerson, W. D. Phillips, and G. K. Campbell, Superflow in a toroidal Bose-Einstein condensate: An atom circuit with a tunable weak link, *Phys. Rev. Lett.* **106**, 130401 (2011).
- [23] K. C. Wright, R. B. Blakestad, C. J. Lobb, W. D. Phillips, and G. K. Campbell, Driving Phase Slips in a Superfluid Atom Circuit with a Rotating Weak Link, *Phys. Rev. Lett.* **110**, 025302 (2013).
- [24] F. Jendrzejewski, S. Eckel, N. Murray, C. Lanier, M. Edwards, C. J. Lobb, and G. K. Campbell, Resistive Flow in a Weakly Interacting Bose-Einstein Condensate, *Phys. Rev. Lett.* **113**, 045305 (2014).
- [25] S. Eckel, J. G. Lee, F. Jendrzejewski, N. Murray, C. W. Clark, C. J. Lobb, W. D. Phillips, M. Edwards, and G. K. Campbell, Hysteresis in a quantized superfluid 'atomtronic' circuit, *Nature (London)* **506**, 200 (2014).
- [26] L. Allen, M. W. Beijersbergen, R. J. C. Spreeuw, and J. P. Woerdman, Orbital angular momentum of light and the transformation of Laguerre-Gaussian laser modes, *Phys. Rev. A* **45**, 8185 (1992).
- [27] Y.-J. Lin, K. Jiménez-García, and I. B. Spielman, Spin-orbit-coupled Bose-Einstein condensates, *Nature (London)* **471**, 83 (2011).
- [28] J.-Y. Zhang, S.-C. Ji, Z. Chen, L. Zhang, Z.-D. Du, B. Yan, G.-S. Pan, B. Zhao, Y.-J. Deng, H. Zhai, S. Chen, and J.-W. Pan, Collective Dipole Oscillations of a Spin-Orbit Coupled Bose-Einstein Condensate, *Phys. Rev. Lett.* **109**, 115301 (2012).
- [29] C. Qu, C. Hamner, M. Gong, C. Zhang, and P. Engels, Observation of Zitterbewegung in a spin-orbit-coupled Bose-Einstein condensate, *Phys. Rev. A* **88**, 021604(R) (2013).
- [30] A. J. Olson, S.-J. Wang, R. J. Niffenegger, C.-H. Li, C. H. Greene, and Y. P. Chen, Tunable Landau-Zener transitions in a spin-orbit-coupled Bose-Einstein condensate, *Phys. Rev. A* **90**, 013616 (2014).
- [31] C. Hamner, C. Qu, Y. Zhang, J. Chang, M. Gong, C. Zhang, and P. Engels, Dicke-type phase transition in a spin-orbit-coupled Bose-Einstein condensate, *Nat. Commun.* **5**, 4023 (2014).
- [32] P. Wang, Z.-Q. Yu, Z. Fu, J. Miao, L. Huang, S. Chai, H. Zhai, and J. Zhang, Spin-Orbit Coupled Degenerate Fermi Gases, *Phys. Rev. Lett.* **109**, 095301 (2012).
- [33] L. W. Cheuk, A. T. Sommer, Z. Hadzibabic, T. Yefsah, W. S. Bakr, and M. W. Zwierlein, Spin-Injection Spectroscopy of a Spin-Orbit Coupled Fermi Gas, *Phys. Rev. Lett.* **109**, 095302 (2012).
- [34] R. A. Williams, M. C. Beeler, L. J. LeBlanc, K. Jiménez-García, and I. B. Spielman, Raman-Induced Interactions in a Single-Component Fermi Gas Near an *s*-Wave Feshbach Resonance, *Phys. Rev. Lett.* **111**, 095301 (2013).
- [35] K. Sun, C. Qu, and C. Zhang, Spin-orbital-angular-momentum coupling in Bose-Einstein condensates, *Phys. Rev. A* **91**, 063627 (2015).
- [36] M. DeMarco, and H. Pu, Angular spin-orbit coupling in cold atoms, *Phys. Rev. A* **91**, 033630 (2015).

- [37] C. Qu, K. Sun, and C. Zhang, Quantum phases of Bose-Einstein condensates with synthetic spin-orbital-angular-momentum coupling, *Phys. Rev. A* **91**, 053630 (2015).
- [38] A. Kumar, N. Anderson, W. D. Phillips, S. Eckel, G. K. Campbell, and S. Stringari, Minimally destructive, Doppler measurement of a quantized flow in a ring-shaped Bose-Einstein condensate, *New J. Phys.* **18**, 025001 (2016).
- [39] E. J. Mueller, Superfluidity and mean-field energy loops: Hysteretic behavior in Bose-Einstein condensates, *Phys. Rev. A* **66**, 063603 (2002).
- [40] G. Watanabe, S. Yoon, and F. Dalfovo, Swallowtail band structure of the superfluid Fermi gas in an optical lattice, *Phys. Rev. Lett.* **107**, 270404 (2011).
- [41] O. Morsch and M. Oberthaler, Dynamics of Bose-Einstein condensates in optical lattices, *Phys. Rev. Lett.* **103**, 140405 (2009).
- [42] N. V. Vitanov, Transition times in the Landau-Zener model, *Phys. Rev. A* **59**, 988 (1999).
- [43] J. Liu, B. Wu, and Q. Niu, Nonlinear evolution of quantum states in the adiabatic regime, *Phys. Rev. Lett.* **90**, 170404 (2003).
- [44] B. Wu and Q. Niu, Nonlinear Landau-Zener tunneling, *Phys. Rev. A* **61**, 023402 (2000).
- [45] R. Wei and E. J. Mueller, Magnetic-field dependence of Raman coupling in alkali-metal atoms, *Phys. Rev. A* **87**, 042514 (2013).
- [46] J. Stenger, S. Inouye, D. M. Stamper-Kurn, H.-J. Miesner, A. P. Chikkatur, and W. Ketterle, Spin domains in ground-state Bose-Einstein condensates, *Nature (London)* **396**, 345 (1998).

Supplementary Materials

Time scale of the adiabatic process

For the adiabatic process given in Fig. 2 (a), V_M should be strong enough to overcome the energy barrier between different $|m\rangle$ states induced by the interaction in order to obtain the desired final state. Therefore a larger V_M is required for stronger interaction with a rough linear relation as shown in the inset in Fig. 5 (a). The red dots show the minimum values of V_M to achieve a smooth transition between different $|m\rangle$ states, where the energy minima for adjacent $|m\rangle$ states are smoothly connected by the adiabatic path.

The required time length of the adiabatic process is closely related to the choice of the adiabatic path in the parameter space, which is determined by V_M and Ω_M . The value of Ω_M can be simply determined by examining the single-particle band structure (or phase diagram). As discussed above, for a given interaction strength, a perfect transition can be realized by slowly tuning the parameters along the path with a large V_M . If the overall time length T is too small, excitations may be created during the process, and consequently, imperfections are introduced in the transition. Fig. 5 (a) illustrates the relations between fidelity and overall time length (T) of the process in Fig. 2 (a). The fidelity is defined as the modulus square of the overlap between the final state and the target state. As T decreases, excitations and their interference with the ground state lead to the fidelity oscillation near $T = 7.5$, and the adiabatic approach breaks down below the time length $T = 7$, where a sudden drop of the fidelity occurs.

For nonlinear quantum problems, the adiabaticity is related to not only the energy-level spacings, but also the fundamental frequencies of periodic orbits around the energy minima. These frequencies can be calculated by linearizing the semi-classical Hamiltonian Eq. 3 around the energy minima. One should expect to have three pairs of frequencies ($\omega_1, \omega_2, \omega_3$), since the degrees of freedom 6 (i.e. the dimension of the phase space is 6). Fig. 5 (b) shows how these fundamental frequencies vary with time during the adiabatic process shown in Fig. 2 (a). The minimum frequency is about 1, indicating that the overall time length should be much longer than 1 to avoid excitations of such periodic orbits. For the processes shown in Fig. 2 (a) and Fig. 3 (d), the energy minimum is far away from any energy maxima in the phase space, therefore the time scales of the adiabatic processes are determined by the fundamental frequencies, as confirmed by the results shown in Fig. 5 (a). For the hysteresis process, the minimum merges with a maximum and both of them disappear after the merging, therefore the periodic orbits may not even exist and these fundamental frequencies lose their physical meanings. In fact, the adiabaticity

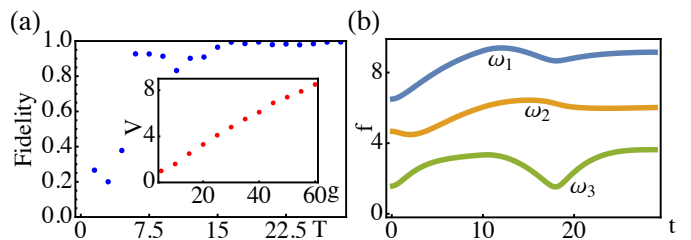


FIG. 5. (color online) (a) Final state fidelity versus the overall time length. The inner panel gives the minimum V_M required to induce the smooth transition for different interaction strength. (b) Fundamental frequencies of the periodic orbits at the energy minimum. For both plots, unmentioned parameters are the same as the transition process in Fig. 2 (a).

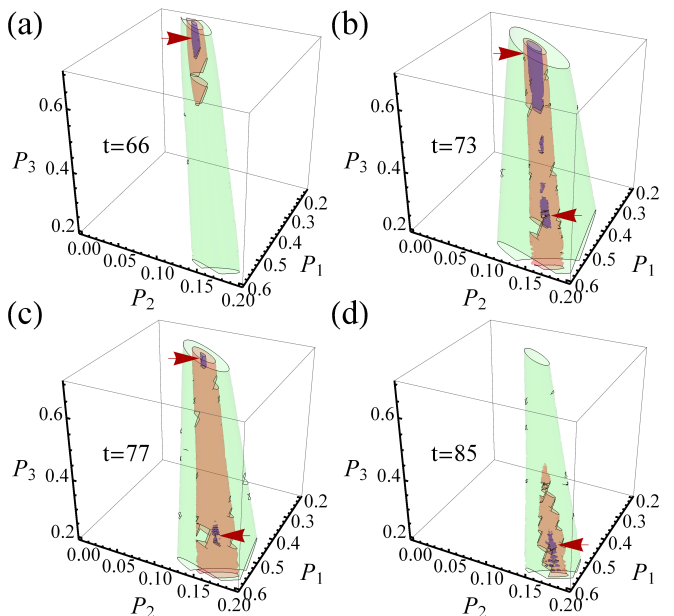


FIG. 6. (color online) Phase space portraits in the subspace spanned by (p_1, p_2, p_3) with $q_1 = 2\pi$, $q_2 = \pi$ and $q_3 = \pi$. Each panel contains three equal-energy surfaces that increase from inner to outside, they are given by $(-10.41, -10.38, -10.3)$ in (a), $(-10.83, -10.8, -10.5)$ in (b), $(-11.1, -11.05, -10.9)$ in (c), and $(-11.64, -11.62, -11.55)$ in (d). The red arrows denote the approximate positions of the minima.

breaks down in the hysteresis process. Nevertheless, our simulation suggests that a longer time is always preferred to get a smoother hysteresis loop.

Energy minima in the phase space

The evolution of energy minima in the phase space are crucial for understanding the adiabatic process. As an example, we consider the hysteresis process discussed in Fig. 3 (c). To visualize the energy minima in the phase space with dimension as high as 6, we first notice that

the minima always satisfy $q_1 = 2\pi$, $q_2 = \pi$ and $q_3 = \pi$. This gives us the possibility to project the whole phase space to a 3D subspace spanned by (p_1, p_2, p_3) . At $t = 66$, there is only one minimum that gives the ground state, as shown in Fig. 6 (a). As we change Ω and V , a second local minimum appears [see Fig. 6 (b) at $t = 73$]. This process is accompanied by the emergence of a local maximum that forms the barrier between the two minima. Though the second minimum may have a lower

energy, the BEC will stay at the first minimum [see Fig. 6 (c) at $t = 77$] until it merges with the maximum and disappears, after which the BEC flows towards the second minimum [see Fig. 6 (d) at $t = 85$]. Those phase-space portraits shown in Fig. 6 provide us a clear picture of the physics behind the swallowtail band structure and the corresponding hysteresis. They confirm our intuitive explanation of the hysteresis phenomena illustrated in Fig. 4(a).